Nano Research
2021, 14(8): 2831–2836
ISSN 1998-0124 CN 11-5974/O4
https://doi.org/10.1007/s12274-021-3295-1

Research Article

Cu_2Sb decorated Cu nanowire arrays for selective electrocatalytic CO_2 to CO conversion

Shiyong Mou[1,§], Yonghao Li[2,§], Luchao Yue[3], Jie Liang[3], Yonglan Luo[2], Qian Liu[3], Tingshuai Li[3], Siyu Lu[4], Abdullah M. Asiri[5], Xiaoli Xiong[1] (✉), Dongwei Ma[6] (✉), and Xuping Sun[3] (✉)

[1] *College of Chemistry and Materials Science, Sichuan Normal University, Chengdu 610068, China*
[2] *Chemical Synthesis and Pollution Control Key Laboratory of Sichuan Province, School of Chemistry and Chemical engineering, China West Normal University, Nanchong 637002, China*
[3] *Institute of Fundamental and Frontier Sciences, University of Electronic Science and Technology of China, Chengdu 610054, China*
[4] *Green Catalysis Center, and College of Chemistry, Zhengzhou University, Zhengzhou 450001, China*
[5] *Chemistry Department, Faculty of Science & Center of Excellence for Advanced Materials Research, King Abdulaziz University, P.O. Box 80203, Jeddah 21589, Saudi Arabia*
[6] *Key Laboratory for Special Functional Materials of Ministry of Education, and School of Materials Science and Engineering, Henan University, Kaifeng 475004, China*
[§] *Shiyong Mou and Yonghao Li contributed equally to this work.*

Received: 26 October 2020 / **Revised:** 11 December 2020 / **Accepted:** 13 December 2020

ABSTRACT

The advancement of cost-effective and selective electrocatalyst towards CO_2 to CO conversion is crucial for renewable energy conversion and storage, thus to achieve carbon-neutral cycle in a sustainable manner. In this communication, we report that Cu_2Sb decorated Cu nanowire arrays on Cu foil act as a highly active and selective electrocatalyst for CO_2 to CO conversion. In CO_2-saturated 0.1 M $KHCO_3$, it achieves a high Faraday efficiency (FE) of 86.5% for CO, at −0.90 V vs. reversible hydrogen electrode (RHE). The H_2/CO ratio is tunable from 0.08:1 to 5.9:1 by adjusting the potential. It is worth noting that $HCOO^-$ product was totally suppressed on such catalyst, compared with Sb counterpart. The improving selectivity for CO could be attributed to the bimetallic effect and nanowire arrays structure.

KEYWORDS

Cu_2Sb, nanowire arrays, electrochemical CO_2 reduction, CO_2 to CO conversion

1 Introduction

The balance of natural carbon cycle has been disrupted by excessive anthropogenic CO_2 emissions from the intensive fossil fuel consumption, leading to both global warming and energy crisis problems [1, 2]. The electrochemical CO_2 reduction (CO_2RR) to carbon-based fuels in aqueous solution appears to be an elegant route for renewable energy conversion and storage, thus achieving a carbon-neutral cycle [3–6]. However, the equilibrium potentials of CO_2RR are very close to the parasitic hydrogen evolution reaction (HER), which diminish the Faraday efficiency (FE) of desired product. Moreover, multiple proton-coupled electron transfer steps highlight the complexity of such reaction, forming a wide range of reduction product mixtures, such as CO, CH_4, C_2H_4, $HCOO^-$, and alcohols [5–8]. Among them, CO holds great importance for the chemical industry since it can be utilized as an important feedstock for the production of carbonbased fuels and useful chemicals via Fischer–Tropsch processes [9–12]. Typically, Au, Ag, and Pd based noble metal catalysts exhibit highly selective electrocatalytic CO_2 to CO conversion in nature [13–15], however, high overpotentials and expensive prices limit the large-scale CO_2RR application. It is thus highly desirable to develop cost-effective, efficient and stable electrocatalysts for such conversion.

Cu is an attractive candidate catalyst for CO_2RR, which, however, suffers from low product selectivity, surface poisoning, and competing HER [6, 16]. Interestingly, recent experimental and theoretical studies suggest that the preparation of bimetallic catalyst is a key tactic to improve CO_2 to CO conversion, benefitting from electronic effects, strain effects and geometric effects, of which catalytic performance is distinct from the pristine catalyst [16, 17]. By alloying, several Au-Cu [18–20], Ag-Cu [21, 22], Pd-Cu [23, 24] bimetallic catalysts have been shown boosted activity for CO production. However, these catalysts involved precious metals, designing a cost-effective bimetallic catalyst should thus be focused on non-noble-metals. Alternatively, the sp-block metal electrocatalysts such as In [25–27], Sn [28, 29], Bi [30], and Sb [31, 32] have previously been identified highly selective for CO_2 to $HCOO^-$ conversion. Encouragingly, the trends of promoted CO formation and HER suppression were observed in In-Cu [33–37], Sn-Cu [38–41] systems. Additionally, recent studies suggested that high surface area Cu nanowire arrays could provide abundant undercoordinated sites, which could affect the catalytic activity and selectivity of CO_2RR [42–44]. It is thus expected that preparing of Sb-Cu bimetallic catalyst with nanowire arrays

Address correspondence to Xiaoli Xiong, xiongxl@sicnu.edu.cn; Dongwei Ma, madw@henu.edu.cn; Xuping Sun, xpsun@uestc.edu.cn

structure would be an ideal solution to enhance CO selectivity.

In this work, we report Cu_2Sb decorated Cu nanowire arrays on Cu foil (Cu_2Sb NA/CF) as a highly active and selective electrocatalyst for CO_2 to CO conversion. In CO_2-saturated 0.1 M $KHCO_3$, it achieves a high FE of 86.5% for CO at −0.90 V vs. reversible hydrogen electrode (RHE), the onset potential observed for CO evolution was −0.50 V vs. RHE. The H_2/CO ratio was tunable from 0.08:1 to 5.9:1 by adjusting the potential. It is worth noting that $HCOO^-$ product was totally suppressed on such catalyst, compared with Sb catalysts (Table S1 in the Electronic Supplementary Material (ESM)). The bimetallic effect and nanowire arrays structure play significant roles in improving selectivity for CO formation.

2 Experimental

2.1 Materials

NaOH, KOH, $(NH_3)_2S_2O_8$, $Cu(NO_3)_2$ and citric acid were purchased from Chengdu Kelong chemical reagent factory. $SbCl_3$ was purchased from Aladdin Ltd. (Shanghai, China). Cu foil was purchased from Wuhan instrument surgical instruments business. Standard gas mixtures were purchased from Dalian special gases Co., Ltd. The water used throughout all experiments was purified through a Millipore system. All chemicals were used as received without further purification.

2.2 Sample preparation

CuO nanowire arrays (CuO NA/CF) were fabricated by annealing $Cu(OH)_2$ nanowire arrays at 180 °C for 1 h in air, in which $Cu(OH)_2$ nanowire arrays were first synthesized on Cu foil by immersing Cu foil into a solution mixture containing 0.13 M $(NH_3)_2S_2O_8$ and 2.60 M NaOH. CuO-derived Cu nanowire arrays (OD Cu NA/CF) were obtained from electrochemical reduction of CuO NA/CF in CO_2-saturated 0.1 M $KHCO_3$ electrolytes at a potential of −1.4 V vs. Ag/AgCl electrode (3 M KCl) for 600 s.

Cu_2Sb were electrodeposited on CuO-derived Cu nanowire arrays to fabricate Cu_2Sb NA/CF at a potential of −1.4 V vs. Ag/AgCl electrode (3 M KCl) for 120 s from 0.4 M citric acid aqueous solution containing 0.025 M $SbCl_3$ and 0.1 M $Cu(NO_3)_2$ [45]. The pH was adjusted to 6 by 5 M KOH. The electrodeposited Cu_2Sb nanowire arrays were then annealed at 220 °C for 5 h under argon. Cu_2Sb nanofilm on Cu foil (Cu_2Sb NF/CF) electrode was fabricated under the same conditions by direct electrodeposition of Cu_2Sb on Cu foil. Sb nanofilm on Cu foil (Sb NF/CF) was fabricated by direct electrodeposition of Sb on Cu foil at a potential of −1.4 V vs. Ag/AgCl electrode (3 M KCl) for 120 s from 0.4 M citric acid aqueous solution containing 0.025 M $SbCl_3$, the pH was adjusted to 6 by 5 M KOH.

2.3 Characterizations

X-ray diffraction (XRD) patterns were obtained from Shimazu XRD-6100 diffractometer with Cu Kα radiation (40 kV, 30 mA). The scanning electron microscopy (SEM) images and energy-dispersive X-ray (EDX) were collected from the field-emission scanning electron microscope (Zeiss Gemini 300, Germany) at an accelerating voltage of 5 and 15 kV, respectively. Transmission electron microscopy (TEM) images were obtained from a Zeiss Libra 200FE transmission electron microscope operated at 200 kV. X-ray photoelectron spectroscopy (XPS) measurements were performed on an ESCALABMK II X-ray photoelectron spectrometer using Mg as the exciting source. Inductively coupled plasma-optical emission spectroscopy (ICP-OES) data were obtained from PerkinElmer optical emission spectrometer (Optima 8000).

2.4 Electrochemical measurements

Electrochemical measurements were performed on a CHI 659E electrochemical analyzer (CHI Instruments, Inc., Shanghai) in a standard three-electrode system using Cu_2Sb NA/CF with an area of 1 cm ×1 cm as working electrode, Ag/AgCl as reference electrode, and graphite rod as counter electrode. A mass flow controller was used to set the CO_2 flow rate at 30 mL·min^{-1}. All experiments were carried out in two-compartment gas-tight H-type cell (50 mL), at ambient conditions. For CO_2 reduction experiments, 30 mL $KHCO_3$ electrolyte (0.1 M) was bubbled with high-purity CO_2 for 30 min before measurement. Polarization curves were obtained using LSV with a scan rate of 2 mV·s^{-1}. All potentials reported in this work were calibrated to RHE, using the following equation

$$E(\text{RHE}) = E(\text{Ag/AgCl}) + (0.197 + 0.059\ \text{pH})\ \text{V} \quad (1)$$

2.5 Quantitative detection of gas products

Detection and quantification of possible gas products (hydrogen, carbon monoxide, carbon dioxide, methane) were performed on a SHIMADZU GC-2014C gas chromatograph system equipped with flame ionization detectors (FIDs), and flame ionization detector with methanizer (FID-methanizer), thermal conductivity detector (TCD) and online auto-sampling system (10 ports VICI valve with 2mL sample loop, packed columns and Aluminum oxide porous layer open tubular capillary column (Rt^{TM}-Alumina, 30 m, 0.32 mm ID)).

2.6 Quantitative detection of alcohols

Gas chromatography (GC-2014C) with headspace autosampler (ColinTech) (HS-GC) was used for the determination of alcohols (methanol and ethanol), the separation was achieved using DB-WAX column (100% polyethylene glycol, 30 m long with 0.53 mm i.d. and 1.0 μm film thickness).

2.7 Quantitative detection of $HCOO^-$

Detection and quantification of $HCOO^-$ was performed on an Metrohm 940 professional ion chromatograph system, in which $HCOO^-$ was separated using an ion exchange column (Metrosep Organic Acids, 250/7.8), following detected with conductivity detectors.

2.8 Calculation of the FE

Calculation of the FE:

$$\text{FE}\% = (n \times z \times F)/It \times 100\% \quad (2)$$

Where: n is the number of moles; z is the number of electrons required for specific product; F is the faradaic constant (96,485 C·mol^{-1}); I is current (A); t is the time required (s).

2.9 Tafel plots calculation

The Tafel plots are employed to evaluate the CO_2RR catalytic kinetics and fitted with the following equation:

$$\eta = b\log j + a \quad (3)$$

3 Results and discussion

The Cu_2Sb NA/CF electrode was fabricated by electrodeposition of Cu_2Sb on OD Cu NA/CF (Fig. 1(a)) [42, 45]. The SEM images of CuO nanowire arrays precursor (Fig. 1(b)) and Cu_2Sb NA/CF (Fig. 1(c)) reveal that Cu_2Sb was successfully electrodeposited onto the surface of Cu nanowires which with diameter range from 100 to 300 nm. The corresponding EDX elemental mapping images of Cu_2Sb NA/CF (Fig. S1 in the ESM) confirm the

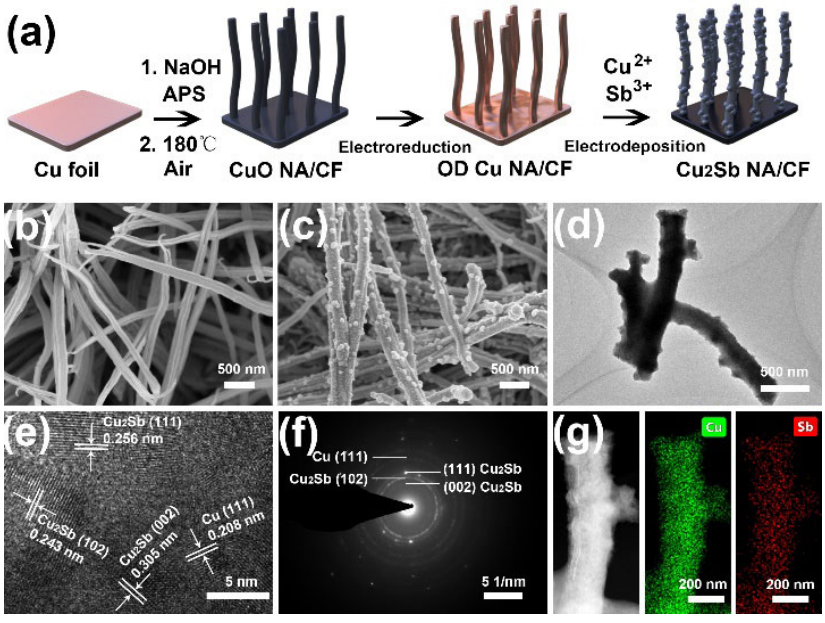

Figure 1 (a) A schematic illustration of the fabrication of Cu_2Sb NA/CF. SEM images for (b) CuO nanowire arrays precursor and (c) Cu_2Sb NA/CF. (d) TEM and (e) HR-TEM images of Cu_2Sb nanowire. (f) SAED pattern taken from the Cu_2Sb nanowire. (g) STEM characterization of Cu_2Sb nanowire, and the corresponding elemental mapping images of Cu and Sb.

existence of Cu and Sb elements, and the obtained atomic ratio of Cu/Sb from EDX spectrum is 2.07 (Fig. S2 in the ESM). Figure 1(d) shows the TEM image of Cu_2Sb nanowire, further confirming its nanowire nature. The high-resolution TEM (HRTEM) image (Fig. 1(e)) taken from Cu_2Sb nanowire reveals clear lattice fringes with interplanar distances of 0.243, 0.256, and 0.305 nm, corresponding to the (102), (111), and (002) planes of Cu_2Sb, respectively.

The selected area electron diffraction (SAED) pattern of Cu_2Sb (Fig. 1(f)) is well consistent with the XRD pattern of Cu_2Sb NA/CF (Fig. 2(a)), in which the diffraction peaks are well matched to the peak positions of Cu_2Sb (JCPDS No. 85-492). The scanning transmission electron microscopy (STEM) image and the corresponding EDX elemental mapping images (Fig. 1(g)) demonstrate the uniform distribution of Cu and Sb. XPS survey spectrum of Cu_2Sb NA/CF (Fig. 2(b)) further reveals the existence of Cu and Sb, moreover, it obtained an atomic ratio of Cu/Sb of 2.15. As indicated by the Cu 2p region in Fig. 2(c), the binding energy at 932.6 eV (Cu $2p_{3/2}$) and 952.4 eV (Cu $2p_{1/2}$) are attributed to metallic Cu [42]. The Sb 3d region is shown in Fig. 2(d), the binding energy at 528.2 eV (Sb $3d_{5/2}$) and 537.5 eV (Sb $3d_{3/2}$) are attributed to metallic Sb. It is possible to identify that the binding energy at 530.1 eV (Sb $3d_{5/2}$) and 539.4 eV (Sb $3d_{3/2}$) are attributed to Sb^{3+}, together with the binding energy of 531.2 eV (O 1s) and wake shake-up satellite peak of Cu $2p_{3/2}$, which were most probably derived from air exposure. All these results manifest the successful fabrication of Cu_2Sb NA/CF electrode by electrodeposition.

To evaluate the electrochemical catalytic CO_2RR performance of Cu_2Sb NA/CF in 0.1 M $KHCO_3$ solution, a three-electrode system was employed, the two-compartment H-type cell was separated by a Nafion 117 membrane. The linear sweep voltammetry (LSV) plots of Cu_2Sb NA/CF in 0.1 M $KHCO_3$ (Fig. 3(a)) shows a much higher current density in the CO_2-saturated solution than that in the Ar-saturated counterpart,

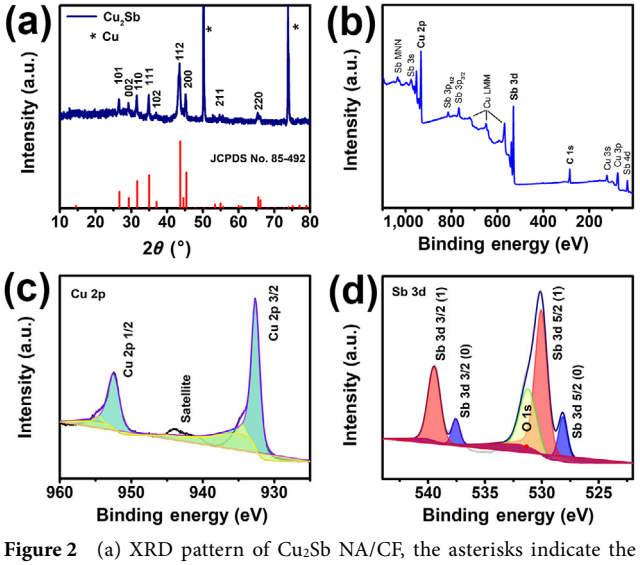

Figure 2 (a) XRD pattern of Cu_2Sb NA/CF, the asterisks indicate the copper substrate diffraction peaks. (b) XPS survey spectrum of Cu_2Sb NA/CF. High-resolution XPS spectra of Cu_2Sb NA/CF in the (c) Cu 2p, (d) Sb 3d regions.

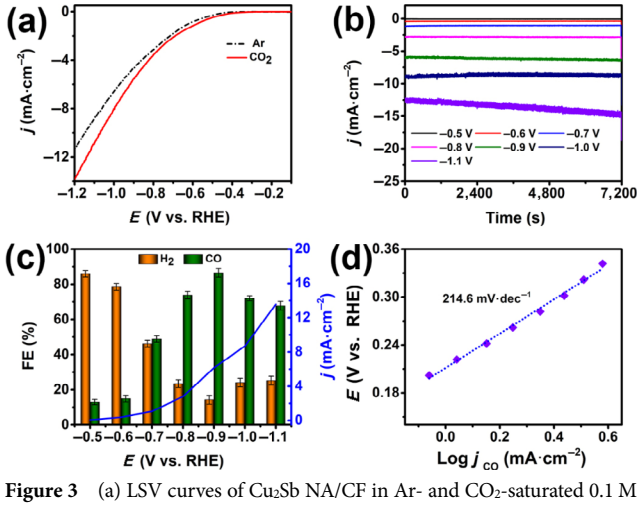

Figure 3 (a) LSV curves of Cu_2Sb NA/CF in Ar- and CO_2-saturated 0.1 M $KHCO_3$ solution. (b) Chronoamperometry curves of CO_2RR over Cu_2Sb NA/CF in 0.1 M $KHCO_3$ solution at different potentials. (c) FEs of CO_2RR on Cu_2Sb NA/CF at different potentials and corresponding current densities. (d) Tafel plots of CO partial current density j_{CO} on Cu_2Sb NA/CF.

manifesting the presence of CO_2 reduction reaction. Accordingly, the potential window from −0.50 to −1.10 V was chosen for CO_2RR investigations. Figure 3(b) shows the constant-potential electrolysis of CO_2 at a series of applied potentials, the steady current densities suggested good electrochemical stability of Cu_2Sb NA/CF catalyst during CO_2RR tests.

To determine the CO_2RR selectivity of Cu_2Sb NA/CF, detection and quantification of reduction products are needed. As shown in Fig. 3(c), the FE for reduction products are plotted at a series of applied potentials. For gaseous products analysis, a tri-channel GC equipped with an online injector is employed. GC analysis results suggest that only CO and H_2 were detected in the gaseous phase. It achieves a maximum FE of 86.5% for CO at −0.90 V with H_2/CO ratio range from 0.08:1 to 5.9:1, which outperforms most of the reported P-block Cu-based bimetallic catalysts (Table S2 in the ESM). For liquid products analysis, a static headspace-gas chromatography (HS-GC) was applied for detection and quantification of alcohols. As shown in Fig. S3(a) in the ESM, no alcohol product was detected.

Additionally, ion chromatography (IC) was employed for the detection and quantification of formic acid, in which $HCOO^-$ was separated using an ion exchange column, following detected with conductivity detector. IC analysis results show that only trace amount (< 0.5 ppm) of $HCOO^-$ was detected on Cu_2Sb NA/CF for each test (Fig. S3(b) in the ESM). Given the fact that Sb nanosheets catalyst have previously been demonstrated with high selectivity for $HCOO^-$ production from CO_2RR [31, 32]. Using Cu nanowires, an FE of approximate 30% for $HCOO^-$ was reached by Ma et al. [42]. In our study, similar results (Fig. 4(a)) were observed on OD Cu NA/CF and Sb NF/CF. It can thus be safely concluded that the CO_2RR selectivity was changed dramatically on Cu_2Sb NA/CF, compared to OD Cu NA/CF and Sb NF/CF counterparts, resulting in the promoted formation of CO. Density functional theory (DFT) calculation results suggesting that on-top Cu was the active site [17]. The presence of $HCOO^-$ producing guest metals do not dramatically impact the electronic structure of Cu, it is more likely a perturbation of surface properties, namely, disrupt active sites for protons while leaving CO active sites unaffected [35, 37, 38]. Tafel plot analysis was performed to gain further insight into the kinetic of CO_2RR on Cu_2Sb NA/CF. Here, a Tafel plots of CO partial current density on Cu_2Sb NA/CF is shown in Fig. 3(d). It exhibits a Tafel slope of 214.6 mV·dec^{-1}, suggesting that the formation of $CO_2^{\bullet-}$ intermediate is the rate-determining step [6].

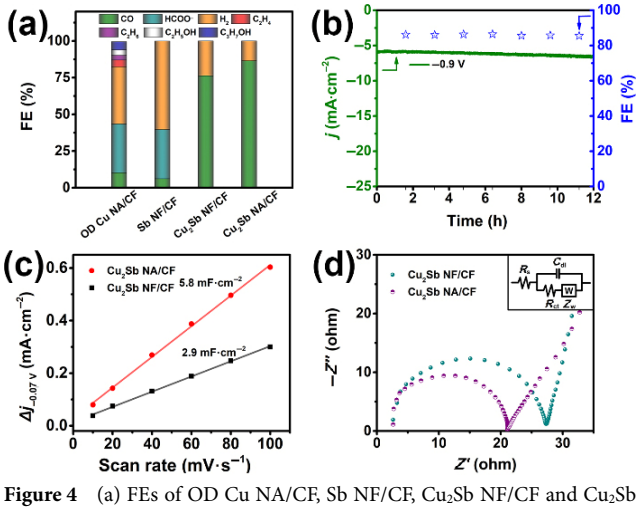

Figure 4 (a) FEs of OD Cu NA/CF, Sb NF/CF, Cu_2Sb NF/CF and Cu_2Sb NA/CF at −0.90 V. (b) Long-term electrochemical stability test of Cu_2Sb NA/CF at −0.90 V for 12 h and FEs for CO. (c) The capacitive current densities at −0.07 V as a function of scan rates for Cu_2Sb NA/CF and Cu_2Sb NF. (d) Nyquist plots of Cu_2Sb NA/CF and Cu_2Sb NF/CF and Randles equivalent circuit (inset).

Control experiments were performed to confirm that CO was generated via electrochemical reduction of CO_2 on Cu_2Sb NA/CF catalyst. We conducted alternate electrolysis cycling tests between Ar- and CO_2-saturated electrolytes (Fig. S5(a) in the ESM), both FEs and partial current densities for CO show no obvious fluctuation, demonstrating the high catalytic stability of Cu_2Sb NA/CF. As shown in Fig. S5(b) in the ESM, no CO product was detected at −0.90 V when purged with Ar. By contrast, when the electrolysis was carried out in a CO_2 atmosphere, the average concentrations of CO that acquired by online GC was 1,318 ppm, which confirms that HCO_3^- is not the immediate source of CO. Supported by these results, it can safely conclude that CO was evolved from the raw CO_2 during CO_2RR test with Cu_2Sb NA/CF catalyst.

To assess the long-term stability of the Cu_2Sb NA/CF catalyst, a 12 h electrolysis was performed at −0.90 V in CO_2-saturated 0.1 M $KHCO_3$. As shown in Fig. 4(b), the Cu_2Sb NA/CF electrode exhibited no obvious fluctuation in current density and the FE for CO was maintained approximately 86.5% during the test, indicating its excellent stability for CO_2RR. Meanwhile, the nanowire arrays structure after long-term stability test were well maintained (Fig. S6 in the ESM). Moreover, XRD pattern (Fig. S7(a) in the ESM), XPS spectra (Figs. S7(b)–S7(d) in the ESM) of Cu_2Sb NA/CF after long-term electrolysis, together with trace amount of Cu and Sb in the electrolyte after long-term stability examined by ICP-OES (Fig. S8 in the ESM) suggest that Cu_2Sb NA/CF exhibits excellent electrochemical stability throughout the CO_2RR test. Previous studies had observed the deactivation of Cu nanowires catalyst during CO_2RR test, due to surface poisoning by the deposited metal impurities which were introduced from electrolyte [46]. Such deactivation was not observed on Cu_2Sb NA/NF, which could be attributed to its good electrochemical durability for the CO_2RR.

To confirm the nanowire arrays morphological effect, CO_2 reduction on Cu_2Sb NF/CF (Fig. S9 in the ESM) were also performed under identical conditions. It can be found that an FE of 76.3% for CO was obtained on Cu_2Sb NF/CF at −0.90 V (Fig. 4(a)), manifesting that Cu_2Sb NA/CF is able to provide enhanced HER suppressing ability, which could attribute to local pH effect [42–44]. It is assumed that the boosted CO_2RR activity is also relevant to the larger electrochemical active surface area (ECSA). To estimate ECSA of Cu_2Sb NA/CF and Cu_2Sb NF/CF, we carried out the measurement of double-layer capacitance (C_{dl}). Figures S10(a) and S10(b) in the ESM, show cyclic voltammograms (CVs) of Cu_2Sb NA/CF and Cu_2Sb NF/CF with various scan rates (10–100 mV·s^{-1}), respectively. Accordingly, as shown in Fig. 4(c), the C_{dl} of Cu_2Sb NA/CF (5.8 mF·cm^{-2}) is higher than that of Cu_2Sb NF/CF (2.9 mF·cm^{-2}), implying a higher ECSA. Furthermore, Nyquist plots (Fig. 4(d)) show that the Cu_2Sb NA/CF has lower charge transfer resistance, which is in accordance with its excellent catalytic performance.

4 Conclusions

In summary, Cu_2Sb NA/CF was successfully fabricated by electrodeposition. As a highly active and selective electrocatalyst for CO_2 to CO conversion, it achieves a high FE of 86.5% for CO, at −0.90 V in 0.1 M $KHCO_3$, the observed onset potential for CO evolution was −0.50 V. The H_2/CO ratio is tunable from 0.08:1 to 5.9:1 by adjusting the potential. Importantly, $HCOO^-$ product was totally suppressed on such catalyst, compared

to Sb counterpart. The bimetallic effect and nanowire arrays structure play significant roles in improving CO selectivity. This work not only provides us an attractive low-cost CO_2RR catalyst, but highlights the significance of bimetallic strategy to tune CO_2RR selectivity.

Acknowledgements

This work was supported by the National Natural Science Foundation of China (No. 22072015) and the Foundation of Sichuan Department of Science and Technology (No. 2017FZ0079).

Electronic Supplementary Material: Supplementary material (EDX elemental mapping; EDX spectrum, HS-GC and IC chromatograms; alternant electrolysis cycling tests between Ar- and CO_2; SEM images, XRD pattern and XPS spectra of Cu_2Sb NA/CF after long-term stability test; ICP-OES analysis; cyclic voltammograms; Tables S1 and S2) is available in the online version of this article at https://doi.org/10.1007/s12274-021-3295-1.

References

[1] Feldman, D. R.; Collins, W. D.; Gero, P. J.; Torn, M. S.; Mlawer E. J.; Shippert, T. R. Observational determination of surface radiative forcing by CO_2 from 2000 to 2010. *Nature* **2015**, *519*, 339–343.

[2] Vitousek, P. M.; Mooney, H. A.; Lubchenco, J.; Melillo, J. M. Human domination of Earth's ecosystems. *Science* **1997**, *277*, 494–499.

[3] Mou, S. Y.; Wu, T. W.; Xie, J. F.; Zhang, Y.; Ji, L.; Huang, H.; Wang, T.; Luo, Y. L.; Xiong, X. L.; Tang, B. et al. Boron phosphide nanoparticles: A nonmetal catalyst for high-selectivity electrochemical reduction of CO_2 to CH_3OH. *Adv. Mater.* **2019**, *31*, 1903499.

[4] Zhao, C. M.; Dai, X. Y.; Yao, T.; Chen, W. X.; Wang, X. Q.; Wang, J.; Yang, J.; Wei, S. Q.; Wu, Y. E.; Li. Y. D. Ionic exchange of metal–organic frameworks to access single nickel sites for efficient electroreduction of CO_2. *J. Am. Chem. Soc.* **2017**, *139*, 8078–8081.

[5] Sun, T. T.; Xu, L. B.; Wang, D. S.; Li, Y. D. Metal organic frameworks derived single atom catalysts for electrocatalytic energy conversion. *Nano Res.* **2019**, *12*, 2067–2080.

[6] Vasileff, A.; Xu, C. C.; Jiao, Y.; Zheng Y.; Qiao, S. Z. Surface and interface engineering in copper-based bimetallic materials for selective CO_2 electroreduction. *Chem* **2018**, *4*, 1809–1831.

[7] Ji, L.; Li, L.; Ji, X. Q.; Zhang, Y.; Mou, S. Y.; Wu, T. W.; Liu, Q.; Li, B. H.; Zhu, X. J.; Luo, Y. L. et al. Highly selective electrochemical reduction of CO_2 to alcohols on an FeP nanoarray. *Angew. Chem., Int. Ed.* **2020**, *59*, 758–762.

[8] Tan, D. X.; Zhang, J. L.; Yao, L.; Tan, X. N.; Cheng, X. Y.; Wan, Q.; Han, B. X.; Zheng, L. R. Zhang, J. Multi-shelled CuO microboxes for carbon dioxide reduction to ethylene. *Nano Res.* **2020**, *13*, 768–774.

[9] Yang, J.; Ma, W. P.; Chen, D.; Holmen A.; Davis, B. H. Fischer–Tropsch synthesis: A review of the effect of CO conversion on methane selectivity. *Appl. Catal. A Gen.* **2014**, *470*, 250–260.

[10] Lee, J. H.; Lee, H. K.; Chun, D. H.; Choi, H.; Rhim, G. B.; Youn, M. H.; Jeong, H.; Kang, S. W.; Yang, J. I.; Jung, H. et al. Phase-controlled synthesis of thermally stable nitrogen-doped carbon supported iron catalysts for highly efficient Fischer-Tropsch synthesis. *Nano Res.* **2019**, *12*, 2568–2575.

[11] Wang, Z. Y.; Yang, J.; Cao, J. B.; Chen, W. X.; Wang, G.; Liao, F.; Zhou, X.; Zhou, F. Y.; Li, R. L.; Yu, Z. Q. et al. Room-temperature synthesis of single iron site by electrofiltration for photoreduction of CO_2 into tunable syngas. *ACS Nano* **2020**, *14*, 6164−6172.

[12] Wang, X. Q.; Chen, Z.; Zhao, X. Y.; Yao, T.; Chen, W. X.; You, R.; Zhao, C. M.; Wu, G.; Wang, J.; Huang, W. X. et al. Regulation of coordination number over single Co sites: Triggering the efficient electroreduction of CO_2. *Angew. Chem., Int. Ed.* **2018**, *57*, 1944–1948.

[13] Chen, Y. H.; Li, C. W.; Kanan, M. W. Aqueous CO_2 reduction at very low overpotential on oxide-derived Au nanoparticles. *J. Am. Chem. Soc.* **2012**, *134*, 19969–19972.

[14] Zhang, Y.; Ji, L.; Qiu, W. B.; Shi, X. F.; Asiri, A. M.; Sun, X. P. Iodide-derived nanostructured silver promotes selective and efficient carbon dioxide conversion into carbon monoxide. *Chem. Commun.* **2018**, *54*, 2666–2669.

[15] He, Q.; Lee, J. H.; Liu, D. B.; Liu, Y. M.; Lin, Z. X.; Xie, Z. H.; Hwang, S.; Kattel, S.; Song, L.; Chen, J. G. Accelerating CO_2 electroreduction to CO over Pd single-atom catalyst. *Adv. Funct. Mater.* **2020**, *30*, 2000407.

[16] Nitopi, S.; Bertheussen, E.; Scott, S. B.; Liu, X. Y.; Engstfeld, A. K.; Horch, S.; Seger, B.; Stephens, I. E. L.; Chan, K.; Hahn, C. et al. Progress and perspectives of electrochemical CO_2 reduction on copper in aqueous electrolyte. *Chem. Rev.* **2019**, *119*, 7610–7672.

[17] Karamad, M.; Tripkovic, V.; Rossmeisl, J. Intermetallic alloys as CO electroreduction catalysts-role of isolated active sites. *ACS Catal.* **2014**, *4*, 2268–2273.

[18] Kim, D.; Resasco, J.; Yu, Y.; Asiri, A. M.; Yang, P. D. Synergistic geometric and electronic effects for electrochemical reduction of carbon dioxide using gold–copper bimetallic nanoparticles. *Nat. Commun.* **2014**, *5*, 4948.

[19] Roy, C.; Galipaud, J.; Fréchette-Viens, L.; Garbarino, S.; Qiao, J.; Guay, D. CO_2 electroreduction at Au_xCu_{1-x} obtained by pulsed laser deposition in O_2 atmosphere. *Electrochim. Acta* **2017**, *246*, 115–122.

[20] Ross, M. B.; Dinh, C. T.; Li, Y. F.; Kim, D.; De Luna, P.; Sargent, E. H.; Yang, P. D. Tunable Cu enrichment enables designer syngas electrosynthesis from CO_2. *J. Am. Chem. Soc.* **2017**, *139*, 9359–9363.

[21] Chen, X. Y.; Henckel, D. A.; Nwabara, U. O.; Li, Y. Y.; Frenkel, A. I.; Fister, T. T.; Kenis, P. J. A.; Gewirth, A. A. Controlling speciation during CO_2 reduction on Cu-alloy electrodes. *ACS Catal.* **2020**, *10*, 672–682.

[22] Wang, Y. X.; Niu, C. L.; Zhu, Y. C. Copper–silver bimetallic nanowire arrays for electrochemical reduction of carbon dioxide. *Nanomaterials* **2019**, *9*, 173.

[23] Ma, S. C.; Sadakiyo, M.; Heima, M.; Luo, R.; Haasch, R. T.; Gold, J. I.; Yamauchi, M.; Kenis, P. J. A. Electroreduction of carbon dioxide to hydrocarbons using bimetallic Cu−Pd catalysts with different mixing patterns. *J. Am. Chem. Soc.* **2017**, *139*, 47–50.

[24] Yin, Z.; Gao, D. F.; Yao, S. Y.; Zhao, B.; Cai, F.; Lin, L. L.; Tang, P.; Zhai, P.; Wang, G. X.; Ma, D. et al. Highly selective palladium-copper bimetallic electrocatalysts for the electrochemical reduction of CO_2 to CO. *Nano Energy* **2016**, *27*, 35–43.

[25] Luo, W.; Xie, W.; Li, M.; Zhang, J.; Züttel, A. 3D hierarchical porous indium catalyst for highly efficient electroreduction of CO_2. *J. Mater. Chem. A* **2019**, *7*, 4505–4515.

[26] Detweiler, Z. M.; White, J. L.; Bernasek, S. L.; Bocarsly, A. B. Anodized indium metal electrodes for enhanced carbon dioxide reduction in aqueous electrolyte. *Langmuir* **2014**, *30*, 7593–7600.

[27] Xia, Z.; Freeman, M.; Zhang, D. X.; Yang, B.; Lei, L. C.; Li, Z. J.; Hou, Y. Highly selective electrochemical conversion of CO_2 to HCOOH on dendritic indium foams. *ChemElectroChem* **2018**, *5*, 253–259.

[28] Won, D. H.; Choi, C. H.; Chung, J.; Chung, M. W.; Kim, E. H.; Woo, S. I. Rational design of a hierarchical tin dendrite electrode for efficient electrochemical reduction of CO_2. *ChemSusChem* **2015**, *8*, 3092–3098.

[29] Chen, Y. H.; Kanan, M. W. Tin oxide dependence of the CO_2 reduction efficiency on tin electrodes and enhanced activity for tin/tin oxide thin-film catalysts. *J. Am. Chem. Soc.* **2012**, *134*, 1986–1989.

[30] Kim, S.; Dong, W. J.; Gim, S.; Sohn, W.; Park, J. Y.; Yoo, C. J.; Jang, H. W.; Lee, J. L. Shape-controlled bismuth nanoflakes as highly selective catalysts for electrochemical carbon dioxide reduction to formate. *Nano Energy* **2017**, *39*, 44–52.

[31] Li, F. W.; Xue, M. Q.; Li, J. Z.; Ma, X. L.; Chen, L.; Zhang, X. J.; MacFarlane, D. R.; Zhang, J. Unlocking the electrocatalytic activity of antimony for CO_2 reduction by two-dimensional engineering of the bulk material. *Angew. Chem., Int. Ed.* **2017**, *56*, 14718–14722.

[32] Jiang, Z. L.; Wang, T.; Pei, J. J.; Shang, H. S.; Zhou, D. N.; Li, H. J.; Dong, J. C.; Wang, Y.; Cao, R.; Zhuang, Z. B. et al. Discovery of main group single $Sb–N_4$ active sites for CO_2 electroreduction to formate with high efficiency. *Energy Environ. Sci.* **2020**, *13*, 2856–2863.

[33] Devi, P.; Malik, K.; Arora, E.; Bhattacharya, S.; Kalendra, V.; Lakshmi, K. V.; Verma, A.; Singh, J. P. Selective electrochemical reduction of CO_2 to CO on CuO/In_2O_3 nanocomposites: Role of oxygen vacancies. *Catal. Sci. Technol.* **2019**, *9*, 5339–5349.

[34] Jang, Y. J.; Lee, J.; Kim, J. H.; Lee, B. J.; Lee, J. S. One-dimensional CuIn alloy nanowires as a robust and efficient electrocatalyst for selective CO_2-to-CO conversion. *J. Power Sources* **2018**, *378*, 412–417.

[35] Jedidi, A.; Rasul, S.; Masih, D.; Cavallo, L.; Takanabe, K. Generation of Cu–In alloy surfaces from $CuInO_2$ as selective catalytic sites for CO_2 electroreduction. *J. Mater. Chem. A* **2015**, *3*, 19085–19092.

[36] Larrazábal, G. O.; Martín, A. J.; Mitchell, S.; Hauert, R.; Pérez-Ramírez, J. Enhanced reduction of CO_2 to CO over Cu−In electrocatalysts: Catalyst evolution is the key. *ACS Catal.* **2016**, *6*, 6265–6274.

[37] Rasul, S.; Anjum, D. H.; Jedidi, A.; Minenkov, Y.; Cavallo, L.; Takanabe, K. A highly selective copper–indium bimetallic electrocatalyst for the electrochemical reduction of aqueous CO_2 to CO. *Angew. Chem., Int. Ed.* **2015**, *54*, 2146–2150.

[38] Sarfraz, S.; Garcia-Esparza, A. T.; Jedidi, A.; Cavallo, L.; Takanabe, K. Cu–Sn bimetallic catalyst for selective aqueous electroreduction of CO_2 to CO. *ACS Catal.* **2016**, *6*, 2842–2851.

[39] Ju, W. B.; Zeng, J. Q.; Bejtka, K.; Ma, H.; Rentsch, D.; Castellino, M.; Sacco, A.; Pirri, C. F.; Battaglia, C. Sn-decorated Cu for selective electrochemical CO_2 to CO conversion: Precision architecture beyond composition design. *ACS Appl. Energy Mater.* **2019**, *2*, 867–872.

[40] Li, Q.; Fu, J. J.; Zhu, W. L.; Chen, Z. Z.; Shen, B.; Wu, L. H.; Xi, Z.; Wang, T. Y.; Lu, G.; Zhu, J. J. et al. Tuning Sn-catalysis for electrochemical reduction of CO_2 to CO via the core/shell Cu/SnO_2 structure. *J. Am. Chem. Soc.* **2017**, *139*, 4290–4293.

[41] Zhao, Y.; Wang, C. Y.; Wallace, G. G. Tin nanoparticles decorated copper oxide nanowires for selective electrochemical reduction of aqueous CO_2 to CO. *J. Mater. Chem. A* **2016**, *4*, 10710–10718.

[42] Ma, M.; Djanashvili, K.; Smith, W. A. Selective electrochemical reduction of CO_2 to CO on CuO-derived Cu nanowires. *Phys. Chem. Chem. Phys.* **2015**, *17*, 20861–20867.

[43] Ma, M.; Djanashvili, K.; Smith, W. A. Controllable hydrocarbon formation from the electrochemical reduction of CO_2 over Cu nanowire arrays. *Angew. Chem., Int. Ed.* **2016**, *55*, 6680–6684.

[44] Cao, L.; Raciti, D.; Li, C. Y.; Livi, K. J. T.; Rottmann, P. F.; Hemker, K. J.; Mueller, T.; Wang, C. Mechanistic insights for low-overpotential electroreduction of CO_2 to CO on copper nanowires. *ACS Catal.* **2017**, *7*, 8578–8587.

[45] Mosby, J. M.; Prieto, A. L. Direct electrodeposition of Cu_2Sb for lithium-ion battery anodes. *J. Am. Chem. Soc.* **2008**, *130*, 10656–10661.

[46] Hori, Y.; Konishi, H.; Futamura, T.; Murata, A.; Koga, O.; Sakurai, H.; Oguma, K. "Deactivation of copper electrode" in electrochemical reduction of CO_2. *Electrochim. Acta* **2005**, *50*, 5354–5369.